Fall 8-21-2019

Modeling Transient Behavior of NiTi Shape Memory Actuator Using Finite Element Analysis: Parametric Study of Rate Effects

Sheymaa Alazzawi
University of Diyala, mahadmyangel@yahoo.com

peter Filip
SIUC, filip@siu.edu

Recommended Citation
Alazzawi, Sheymaa and Filip, peter. "Modeling Transient Behavior of NiTi Shape Memory Actuator Using Finite Element Analysis: Parametric Study of Rate Effects." *Results in Materials* 1 (Fall 2019). doi:https://doi.org/10.1016/j.rinma.2019.100015.

Results in Materials 1 (2019) 100015

Contents lists available at ScienceDirect

Results in Materials

journal homepage: www.journals.elsevier.com/results-in-materials

Modeling the transient behavior of the NiTi shape memory actuator using finite element analysis: Parametric study of the rate effects

Sheymaa Alazzawi [a,b,*], Peter Filip [a]

[a] Department of Mechanical Engineering and Energy Processes, Southern Illinois University, Carbondale, IL, 62901, USA
[b] Department of Mechanical Engineering, University of Diyala, Diyala, 10061, Iraq

ARTICLE INFO

Keywords:
Shape memory alloy
Actuator
Finite element analysis
Rate effects

ABSTRACT

Finite element simulation is presented to study the rate effects of the shape memory response of bent NiTi wire "C-shaped" exposure to load. A three-dimensional constitutive model for shape memory alloys proposed by Auricchio is implemented in the built-in library of Ansys Workbench 18.2 to capture the shape memory behavior of three different NiTi alloys that are subjected to different thermomechanical treatments. The quasi-static (slow) loading rate and the dynamic (fast) loading rate have been applied isothermally or at adiabatic conditions. Other models assumed the classical shape memory stress-strain behavior, but the realistic behavior of the NiTi SMA is different. The NiTi SMA is influenced by its microstructural changes, such as internal defects, grain size, chemical compositions, content of dislocations and density; all these effects should be added when modeling, which has been considered in this study. The results showed a significant effect of the dynamic loading of NiTi on decreasing the recoverable strain. As a result, it could be expected that the actuator lifetime could be reduced when a rapid, as opposed to a slow, loading rate is adopted. Inhomogeneity of stresses and deformations after loading can cause irreversible plastic deformation. The complete deformation recovery is noticed in the reorientation scenario, unlike in the SIM scenario, which exhibits unrecoverable deformation. Experimental validation is done by comparing the macroscopic displacement of the bent NiTi actuator with the model results, which shows good agreement.

1. Introduction

Developing high-quality and "high-density" functional smart applications overcomes some of the technical and commercial restrictions that are associated with system components, such as undesirable weight and volume issues. The available space, operating environment, response time and affordable cost shall be minimized to increase efficiency [1]. In the transportation industry, using smart systems reduces fuel consumption and improves performance.

Among the numerous actuation systems that are used in the industry, shape memory alloys (SMAs) are viewed as one of the most promising "smart materials" [2]. Shape memory alloys (SMAs) can recover their original shape by simple heating after being mechanically deformed at a sufficiently low temperature (the shape memory effect) or allow for large recoverable strains (superelasticity) at a semiconstant temperature above critical temperatures [3]. These unique properties, which are related to the solid-solid martensitic phase transformation from a high-symmetry phase (austenite) to a low-symmetry phase (martensite), encourage their potential use in a wide range of mechanical, aerospace and biomedical fields [2,4].

In the bias reset mechanism, the spring produces a variable force level, while the weight produces a constant force level [5] that is desirable to keep the stress at a constant level and prevents the functional problem during cycling, such as the shift in the transformation temperatures. Therefore, a constant force level is considered in this study. Under pure tension or compression load, high forces but relatively small displacements can be reached. However, larger displacements are achieved under torsion or bending loads [5]. Therefore, designing bent geometry, such as the proposed "C shape" that dominates bending loads to achieve large-strain capabilities is targeted in this effort. This type of bent shape can be used for cyclic applications and where net displacement delivery is required, such as the valves.

The deformation behavior, shape memory parameters, and corrosion behavior of NiTi SMAs are considerably affected by their microstructure resulting from chemical composition, grain size and/or dislocation or defect density, and the presence of coherent precipitates [6]. The fact

* Corresponding author. Mechanical Engineering Department and Energy Processes, Southern Illinois University of Carbondale, Carbondale, IL, 62901, USA.
E-mail addresses: sheymaa78@siu.edu (S. Alazzawi), filip@siu.edu (P. Filip).

https://doi.org/10.1016/j.rinma.2019.100015
Received in revised form 27 July 2019; Accepted 30 July 2019
Available online 21 August 2019

that any 0.1% change of the Ni content causes a change in the transformation temperature by approximately 10 °C in binary NiTi alloys shows the significant effect of the chemical composition on the NiTi SMAs performance [7].

Work hardening of NiTi SMAs and the related introduction of defects also causes changes in the transformation temperatures and can lead to an increase in generated stresses when compared to the annealed NiTi SMAs with larger grains and lower dislocation density [6]. Transformation stress dependence on the temperature follows the Clausius-Clapeyron relationship [6]:

$$\frac{d\sigma_{SIM}}{dT} = \frac{\Delta H}{\varepsilon_{tr} - T_o}, \quad (1)$$

where σ_{SIM} is the critical stress at which the stress-induced martensitic phase transformation starts, ΔH is the transformation enthalpy, T_o is the equilibrium temperature, and ε_{tr} is the transformation plasticity. The increase of σ_{SIM} with increasing loading temperature is typically accompanied by a decrease in the transformation plasticity ε_{tr} [6,8].

The thermomechanical response of the NiTi wire could be accurately defined in the stress-temperature-transformation plot, as shown in Fig. 1. As a result of the transformation between two phases, the NiTi wire can exhibit two unique behaviors, superelasticity (PE) when loading above A_f up to M_d , and the shape memory effect when loading under M_f . A subsequent heating combination of behaviors can be achieved when loading between M_f and A_f temperatures [2]. The four-transformation temperatures (i.e., M_f , M_s A_s, A_f) are stress dependent, as shown schematically in Fig. 1. The inclined lines in the plot, which cross the temperature axis at either M_s or A_f temperature, show the different critical stresses-temperature dependences the material reaches at different loading conditions.

When loading the NiTi wire at any temperature and reaching the intersection point with the unrecoverable plastic deformation line σ_p , the strain is unrecoverable, because σ_p, which represents the applied stress, leads to the generation of dislocations and irreversible plastic deformation. Cooling the material to a T lower than A_f , then loading at any temperature between A_f and M_s, leads to a stress-induced martensite formation after reaching the critical stress σ_{SIM} , which is schematically represented by line (M_s -2-3) and satisfies eq. (2). The σ_{SIM} is required to form a stress-induced martensite from austenite, which is relevant for the targeted "transformation scenario." To obtain as low critical stress σ_{SIM} as possible, the memory material should be loaded as close to M_s (schematically marked as point 6 in Fig. 1) as possible.

The second targeted stress shown on the plot is the reorientation stress σ_M^r , which is necessary for the reorientation of the present, randomly oriented self-accommodated and twinned martensitic variants. To reach this condition, the material should be loaded after cooling from austinite to a temperature below M_f. To exhibit as low critical stress σ_M^r as possible, the material should be loaded after heating from below M_f to a temperature as close as possible to A_f, as marked by point 7 in Fig. 1. At the end of the loading process, all martensite variants can be detwinned. The targeted stress-induced martensite scenario (I) happens when cooling the three respective alloys A, B, and C, below A_f and loading above M_s . For modeling, the same temperature interval (ΔT_I) was used for the three alloys.

σ□M is stress that is necessary for the reorientation of twinned martensitic variants; σ_{SIM} is the critical stress that is required to form stress-induced martensite from austenite; and σ_p is stress leading to the generation of dislocations and irreversible plastic deformations.

Therefore, the loading by force of 1.3 N occurred at $T_{SIM} = M_s + \Delta T_I$, as marked by point 5 in Fig. 1. Then, the loaded NiTi element is heated from a temperature corresponding to point 5 to a temperature above A_f^σ (shown in Fig. 1), which ends the first thermomechanical cycle. The subsequent thermomechanical cycle starts after cooling the loaded NiTi below point 8, where the stress-induced martensite phase transformation occurs again to repeat the first cycle.

Similarly, in the reorientation scenario, the alloys were cooled from austenite below M_f by the same temperature interval (ΔT_{II}) and were subsequently loaded by a force of 1.3 N. Hence, the loading occurs at

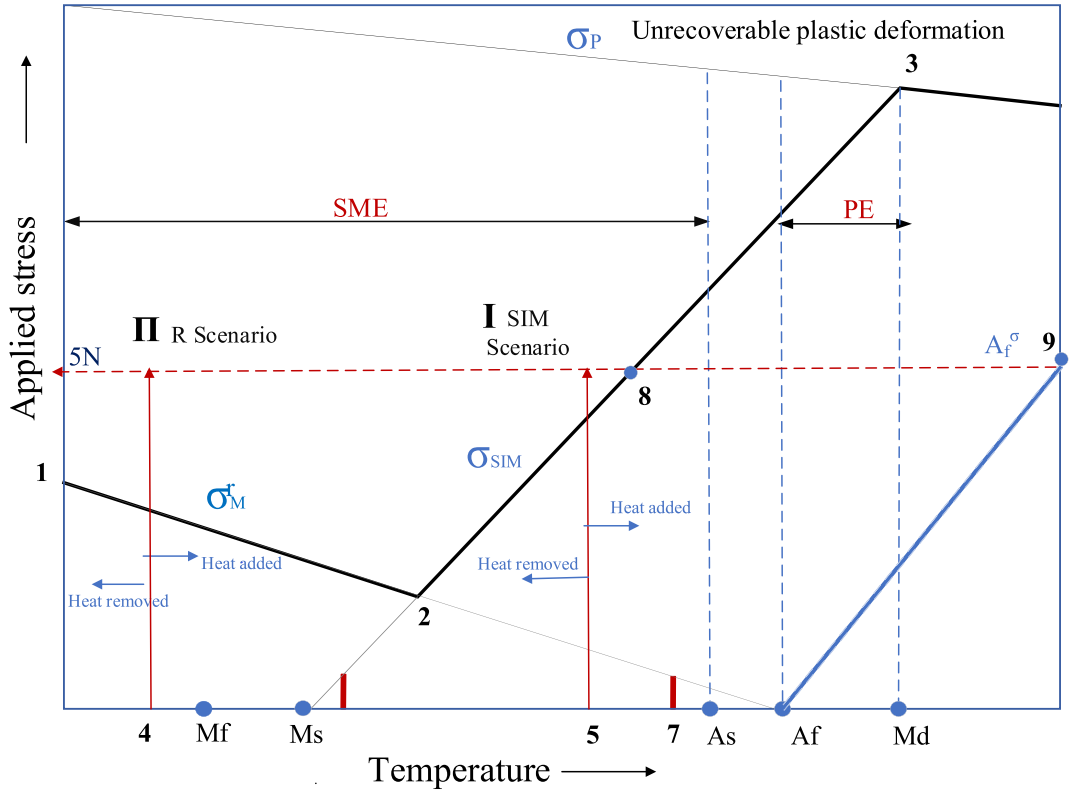

Fig. 1. Critical yielding stress dependence on temperature.

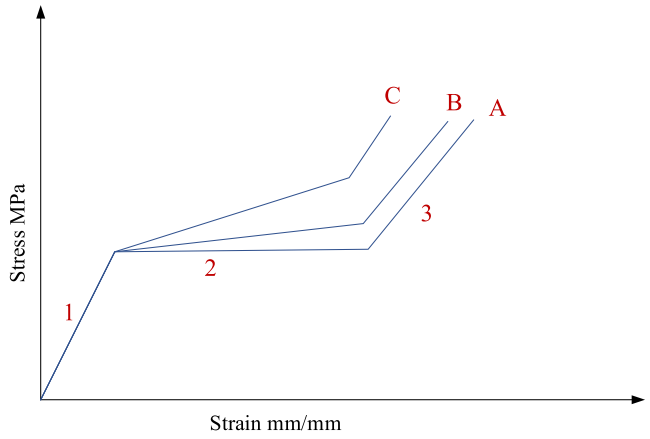

Fig. 2. The stress-strain curves of deferent loading parts in addition to different "hardening" slopes.

temperature $T_R = M_f$ - ΔT_{II} , as marked by point 4 in Fig. 1. Heating the loaded NiTi element from a temperature corresponding to point 4 to a temperature above A_f^σ (shown in Fig. 1) represents the first thermo-mechanical cycle. The following cycle starts when the loaded NiTi element cools down below point 8, where the stress-induced martensite phase transformation occurs.

The stress strain curve has three parts, as shown in Fig. 2; the initial loading up to critical stress, followed by stress-strain dependences that are linked either to stress-induced transformation or reorientation with different slopes depending on the microstructure [4] and, finally, the loading preferentially reoriented martensite. The initial loading slope, as marked by 1 in Fig. 2, represents the "modulus of elasticity" of the self-accommodated martensite or austenite, depending on either initial phase. The third loading slope, as marked by 3 in Fig. 2, represents only the "modulus of elasticity," which is preferentially reoriented martensite, while the second loading slope, as marked by 2 in Fig. 3, gives most of the recoverable strain. It has a different slope, if compared with slopes 1 and 3, and characterizes "hardening" [4]. Although influenced by present dislocation, this "hardening" slope represents either reorientation or the stress-induced martensite (SIM) process. However, when more dislocation is present in the structure, the "hardening" slope is steeper and shorter, as shown by curve C in Fig. 2, and when less dislocation is generated, the hardening slope is lower, as shown by the curve. When there are no dislocations generated, the "hardening" slope is ideally flat, as shown by curve A in Fig. 2.

Combination of work hardening in the austenitic (high temperature) phase followed by annealing has been widely studied to improve the NiTi fatigue performance [7].

Filip and Mazanec presented experimental work on three NiTi alloys with different chemical compositions (Ti-49.5 at. %Ni, Ti-50.4 at. %Ni and Ti-50.8 at. %Ni), which were subjected to different thermo-mechanical treatments. Part of the NiTi SMA alloys were work-hardened by cold-rolling, while the rest of the work-hardened specimens were further subjected to annealing at 400 and 500 °C/1 h/water, respectively. Subsequently, the tensile test was performed at different loading temperatures T, while NiTi SMA were in either the fully martensitic phase (T˂ M_f for specimen A) or the fully austenitic phase (A_s ˂ T˂ A_f and T˃ A_f for specimens B and C, respectively) [8].

The work-hardened specimens A exhibited higher critical stresses σ_{SIM} for SIM phase transformation or σ_M^r for reorientation, a larger slope $\frac{d\sigma}{d\varepsilon}$ in the stress-strain dependence (hardening parameter) and the higher "elastic moduli" than that of annealed specimens [8]. Upon loading of the work-hardened B samples, the stress-induced martensite formed at a higher critical stress compared with the critical stress that was observed for the work-hardened A specimens. The critical stress of the annealed B samples is not higher when compared with the critical stress of the work-hardened B samples and the annealed A specimens. An excellent shape recovery occurs after unloading of the work-hardened B specimens [8].

During phase transformation, latent (transformation) heat is either generated (austenite to martensite) or absorbed (in reverse transformation martensite to austenite) [9]. Depending on the circumstances, this "heat generation" can affect the actual material temperature and, as a result, its response to mechanical stimuli. This is an indicator of strong thermomechanical coupling, which was emphasized in earlier research [10,11].

Auricchio and Sacco developed a finite strain model, including thermomechanical coupling, to simulate the mechanical behavior of the superelastic SMAs under different loading conditions for isothermal and adiabatic cases [10]. The rate dependent behavior of SMA rods during loading-unloading were studied by Auricchio et al. [12] and Lagudous et al. [11], who assumed that the temperature distribution of a small cross-section wire is uniform.

A high strain rate process (dynamic loading) does not allow the material to exchange heat with its surroundings. Consequently, the SMA device works under adiabatic conditions. While in the case of the low strain rate (quasi-static loading), heat exchanges sufficiently fast with the surroundings, which allows the SMA device temperature to be identical with the ambient temperature and, as a result, such loading can be considered to be an isothermal process. This assumption was further adjusted by other experimental and numerical works, which proved the strong impact of the SMA element size, as well as the ambient conditions in addition to the loading rate, in deciding whether the actual system will be an adiabatic or isothermal device [12,13].

Nemat-Nasser et al. presented an experimental work to test a cylindrical superelastic NiTi SMA under high and low strain rates [14]. They concluded that the annealing temperature has considerable impact on the dissipated energy and on the transformation stress. As a consequence of annealing, Nemat-Nasser et al. observed high sensitivity of the superelastic behavior to the changing temperature and less relevant impact of the strain rates.

Majority of models consider perfect behavior of specific condition (well-annealed) materials such as Mazanec, Nemat-Nasser, Miyazaki and many more who only showed the linear behavior of the stress-strain slope with the x-axis. However, the materials could change their properties in the course of their applications, or they intentionally modified by introducing defects which causes shifting in the transformation temperatures, the critical stress, the recoverable strain in addition to the change in the stress-strain slope. In this study, we considered present of these defects in the NiTi microstructure which can be generated during

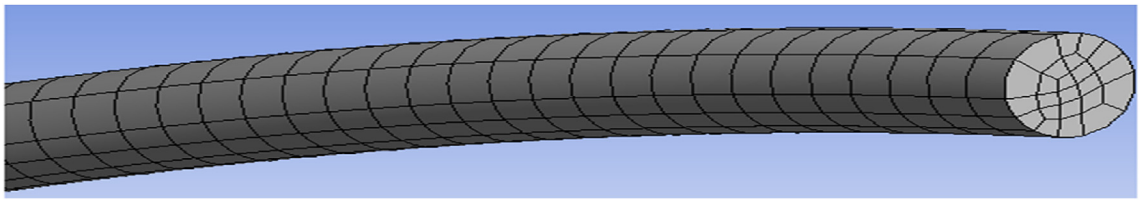

Fig. 3. Detail of the NiTi wire meshing model using Ansys Workbench 18.2.

Table 1
Mechanical and thermal properties of the NiTi wire that was used in the Ansys model [8,20,21].

Property (unit)	Specimen A	Specimen B	Specimen C
"Elastic modulus" of austenite (MPa) [7]	51,700	51,700	51,700
Elastic modulus of martensite (MPa) [7]	42,000	43,000	46,000
Poisson's ratio [18]	0.3	0.3	0.3
Hardening parameter, H (MPa) [7]	85	106	145
Elastic limit, R (MPa) [7]	192	177	167
Temperature scaling parameter, β (MPa·°C^{-1}) [7]	5.6	5.6	5.6
Maximum strain (mm/mm)	0.04	0.04	0.04
Loading temperature, $T_{SIM} = M_s + \Delta T_I$, $T_R = M_f$ - ΔT_{II} (°C)	45	−20	−100
Density (kg.m^{-3}) [19]	6450	6450	6450
Thermal conductivity (W/m. °C) [19]	18	18	18
Average heat capacity (J/kg. °C) [19]	320	320	320
Martensite finish temperature M_f(°C) [7]	50	−15	−95
Martensite start temperature M_s(°C) [7]	85	10	−65
Austenite start temperature A_s(°C) [7]	90	25	−55
Austenite finish temperature A_f(°C) [7]	115	40	−15

repeated use and their impact on the material properties and nobody paying attention to that.

In another effort, Grabe et al. who conducted experiments with superelastic SMA wires, showed the effect of loading rates, which disappeared completely when the test temperature was kept constant [15]. This would lead to the conclusion that the "loading rate" dependence of deformation behavior and observed changes in memory behavior is, in fact, due to the temperature effect.

Another study focused on the localization phenomenon, which occurs during the phase transformation due to lattice deformation and leads to the formation of "*transformation bands.*" He and Sun found that the fluctuation of the local temperature strongly shifts the localized transformation characteristics (see eq. (1)) and leads to the formation of transformation bands [16]. Therefore, the transformation behavior highly depends on the speed of the heat releasing (strongly affected by loading rates) and heat removal by conduction and convection [17].

Depriester et al. developed one-dimensional thermomechanical coupling of superelastic SMAs to simulate the localization phenomenon in more detail [17]. They proved that there was a strong relation between the number of transformation bands and the strain rate.

In a recent finite element analysis using ABAQUS, a three-dimensional model was developed by Yu et al. to simulate the strain and stress distributions during high strain rates of compressed austenitic NiTi SMA [18]. They noticed an increase in the slope of the stress-strain curve during the phase transformation at high strain rates.

When developing models, the majority of researchers focused more on quasi-static loading and on the superelastic NiTi and less on the shape memory effect. Compared to the models that were previously developed for dynamic and quasi-static loading of austenitic NiTi SMAs, a transient thermal-structural simulation for varying rates of deformation of both austenitic and martensitic structures and with and without an adiabatic effect has not been developed yet. Therefore, this work aims to develop this type of simulation and to precisely analyze the coupled thermomechanical behavior of the shape memory effect in NiTi SMA wires that are subjected to dynamic and quasi-static loading conditions during the austenitic phase (M_s ˂ T˂ A_s) and in the martensitic phase (T˂ M_f), respectively. Ansys 18.2 is used to design and simulate this behavior under different loading and boundary conditions.

In the traditional approach, there are two ways to achieve thermomechanical coupling. First, the user tends to use Ansys parametric design language (APDL) command in the structural analysis system to include thermal loads or the boundary conditions using the so-called *direct coupling* method. Second, the user tends to solve the thermal model initially by using the thermal analysis system and then feeds the results into the structural analysis system using so-called *nondirect coupling.*

In the numerical simulation presented in this paper, the new direct coupled field physics approach was used to allow thermomechanical coupling of the material. This approach makes it easier to include thermal loadings and boundary conditions at the same time, in combination with the structural loads and boundary conditions of the structural analysis system. In addition, this approach combines the structural and thermal analysis systems together in one mesh, which makes the results more precise than that of the traditional approach.

It is assumed that the transformation temperatures with the material properties that were obtained for these alloys and are listed in Table 1, are sufficient to support the model, which will identify the deformation behavior of each alloy. To verify this assumption, a macroscopic displacement comparison of the "C-shaped" NiTi wire between the simulation and experimental work is performed.

2. Materials and methods

Table 1 summarizes the material properties and the compositions of three binary NiTi alloys, which were thermomechanically treated as described in Filip and Mazanec's article [8]. The behavior of the "C-shaped actuators" composed of these alloys is simulated under loading at high and low strain rates using ANSYS Workbench 18.2 (the student version). A three-dimensional constitutive model proposed by Auricchio, which is already implemented in the built-in library of ANSYS Workbench 18.2, is used. A transient structural analysis allowed for the macroscopic behavior of the NiTi actuator to be modeled, and this analysis was coupled with a thermal structural analysis by using the "coupled field physics application" to include the thermal loads and boundary conditions.

A coupled-field analysis is useful for solving problems wherein the coupled interaction of the phenomena from various disciplines of physical science is significant, such as the usual influence of temperature-dependent material properties [19]. This unified analysis combines the effects of interrelated physical phenomena and allows for structural-thermal coupled capabilities, which in advance allows for the thermal stress analysis to be conducted [19]. There are two ways to do this type of coupling, using the direct (strong) and the sequential (weak) coupled-field approach [19]. The presented work depends on the direct coupling approach in solving one set of equations with the degree of freedom (DOF) from multiple fields using specialized coupled-field elements in one mesh, which makes the results more precise and reduces possible errors [19]. Sequential coupling solves the equations sequentially in multiple analyses and in multiple meshes. The results of one analysis are applied as loads in other analyses, which make the percentage of errors higher than that of direct coupling [19].

The behavior of a 235.5 mm-long NiTi wire, with a diameter of 1.5 mm, and a "C-shaped actuator" is modeled using a solid element (226) in meshing the wire structure with 6440 elements and 24,442 nodes in the case of thermal and structural coupling and with a solid element 186 in the case of loading at a constant temperature (Fig. 3). To reach the nonlinear convergence easily, a small division of the time steps is used with a quadratic element order and a fine relevance center. The structural and thermal loads and boundary conditions are applied alternately.

The NiTi SMA actuator is fixed at one end, A, using a remote displacement support and is loaded either dynamically or quasi-statically at the free end, B, by applying 1.3 N force, as shown in Fig. 4. This force application leads either to the phase transformation of the austenite to the detwinned martensite, the "stress-induced scenario," or to a reorientation that is self-accommodated to detwinned martensite, the "reorientation scenario," depending on the relative position of the loading temperature and transformation temperature of loaded NiTi alloys. In quasi-static loading, the strain rate was set to $5 \times 10^{-5} s^{-1}$ at three different temperatures of 88 °C, 22 °C, −60 °C (M_s ˂ T˂ A_s) , for the

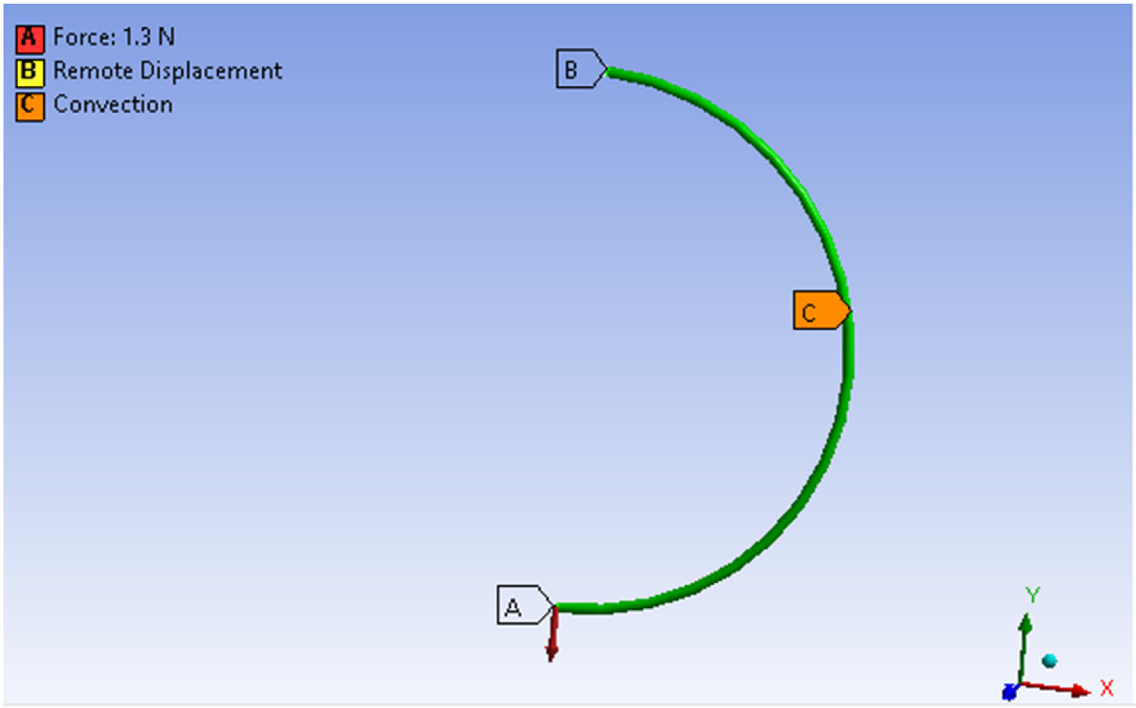

Fig. 4. The "C-shaped" NiTi wire load, supports and boundary conditions during dynamic and quasi-static loading.

respective model alloys A, B and C, whereas in dynamic loading, the strain rate was set to 0.2 s^{-1} at the same temperatures. The same supports, boundary conditions and two different loading rates were also applied for the model alloys A, B and C, which were loaded in the martensitic phase, (when T‹ M_f) at the three respective temperatures of 40 °C, −20 °C and −100 °C for the three model alloys A, B, and C.

When modeling the relation of the NiTi alloys by using ANSYS solving, the equation that was derived from the first law of thermodynamic ignoring radiation was applied as follows [9]:

$$\rho\dot{u} + q - \sigma\dot{\varepsilon} - \rho\dot{g} = 0 \tag{2}$$

In this equation, ρ is the mass density, $\dot{u}$ is the internal energy rate per unit of mass, and $\dot{\sigma}$ and $\dot{\varepsilon}$ are the stress and the strain rate, respectively. The parameter q represents the heat flux and $\dot{g}$ includes the internal heat generation rate due to the above-mentioned phase transformation process, if present.

The generated or released energy in the loaded wire comes mostly in the form of latent heat due to the phase transformation, so the last term in eq. (2) was neglected if there was no phase transformation, and the deformation is linked with a reorientation of the self-accommodated twinned martensite. The stress power term ($\sigma\dot{\varepsilon}$) in eq. (2) can also be neglected for the quasi -static loading scenario, but it has to be considered in the dynamic loading situation.

Based on Fourier's law, the heat flux can be calculated as follows:

$$q = -k\left(\frac{\partial^2 T}{\partial x^2} + \frac{\partial^2 T}{\partial r^2} + \frac{\partial^2 T}{\partial \theta^2}\right), \tag{3}$$

where k is the thermal conductivity, x represents the longitudinal axis, and r is the radial axis of the wire. Because of the symmetry of the circular of NiTi wire, $\frac{\partial^2 T}{\partial \theta^2}$ is considered to be 0 in eq. (3).

The convection boundary conditions can be given as follows:

$$k\frac{\partial T}{\partial r} = h(T_\infty - T), \tag{4}$$

where h is the heat transfer coefficient, T_∞ is the ambient temperature and T is the actual wire temperature.

The heat generation is calculated from the following equation:

$$\mathrm{T}(r) = \dot{g}\left(D^2 - r^2\right) / 2\mathrm{k}, \tag{5}$$

where T(r) is the maximum temperature of the wire.where H is a material parameter defining the slope of the linear stress-transformation strain relation, R is the starting or the yield stress of material detwinning and β is a material parameter related to the dependence of the stress-induced transformation on the temperature [20].

The thermomechanical parameters mentioned in Table 1, such as the "elastic moduli" of austenite and martensite, Poisson's ratio, the elastic limit, and the temperature scaling parameter, were obtained from Ref. [8], while other physical and thermal properties, such as density, thermal conductivity and average heat capacity, were obtained from Ref. [21]. The transformation temperatures were adopted from Ref. [8], which represents characteristics of three alloys with different chemical compositions and thermomechanical treatments.

3. Results and discussion

Two scenarios have been modeled, i.e., stress-induced martensite (SIM) and reorientation (R) scenarios. In both scenarios, dynamic and quasi-static loading was applied. The SIM scenario is typical by the phase transformation from austinite to martensite; this transformation always generates latent heat, as represented by $\dot{g}$ in eq. (2). This heat could be dissipated (isothermal), or it could be kept in the system (adiabatic) depending on the loading rate (i.e., static or dynamic). While in the reorientation scenario, which happens only in the first cycle, there is no phase transformation that occurs, which means that no heat is added (i.e., $\dot{g} = 0$ in eq. (2)) to the system. As a result, similar isothermal and adiabatic behaviors were noticed when loading the material dynamically and statically. It is also important to mention that, after the end of the first thermomechanical cycle, the reorientation scenario is followed by stress-induced martensite to start the second and subsequent thermomechanical cycles.

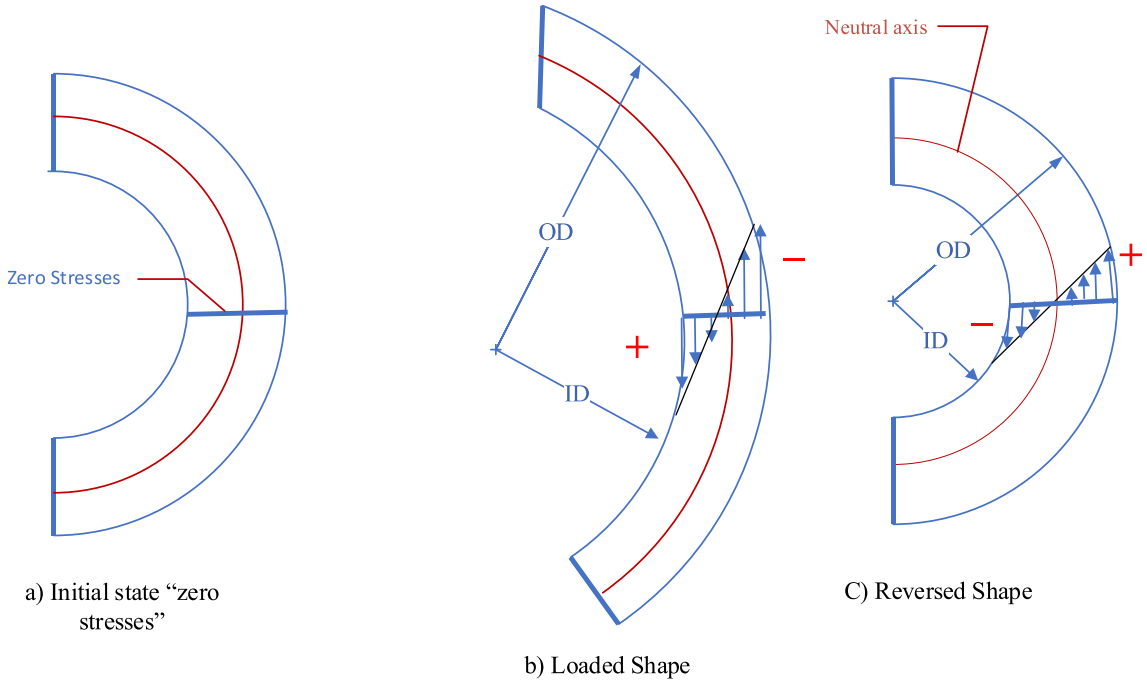

Fig. 5. Schematics of "C-shaped" NiTi memory element with stress distribution in the initial stage (a), after loading at a lower temperature (b), and shape recovery upon heating to T> A_f^{σ}(c).((c.

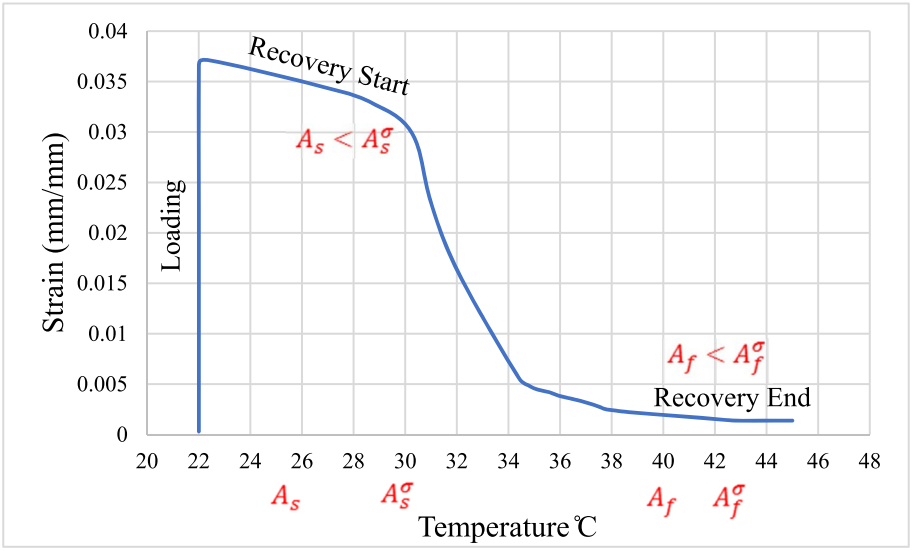

Fig. 6. The temperature-strain curve of the "C-shaped" NiTi element during quasi-static loading and the strain recovery process in the stress-induced martensite scenario.

3.1. Quasi-static loading and the stress-induced martensite phase transformation scenario

In this case, the loaded "C-shaped" articles are in a fully austenitic state after being cooled from the above A_f temperature to the loading temperature $T_{SIM} = M_s + \Delta T_1$. The loading temperatures were 88 °C, 22 °C and −58 °C for specimens A, B, and C, respectively. The strain rate is an important factor affecting the deformation behavior, and it is the ratio of the loading velocity (V) to the initial length of the wire (L) before bending into a "C shape." Moreover, the heat convection is activated in Ansys and is applied on the circumferential surfaces of loaded wire, which leaves the entire wire in isothermal conditions. Since the NiTi wire is surrounded by an ambient air, the heat transfer coefficient (h) is considered to be 5 W/m^2.°C, as established in Mirzaeifar et al. [9].

In the stress-induced scenario, the loading/stressing process of the bent "C-shaped" NiTi wire starts with an elastic deformation of austenite and, once the load reaches the critical limit σ_{SIM} (Fig. 1), the formation of stress-induced martensite begins. With respect to the maximum stress, only variants of martensite grow, and this results in the formation of detwinned martensite. This is linked to large transformation plasticity followed by elastic straining after the transformation plasticity is exhausted.

The deformation behavior during the phase transformation from austenite to stress-induced detwinned martensite follows the Clausius Clapeyron equation (eq. (1)) as shown by line Ms-2-3 in Fig. 1. Any increase of the critical stress σ_{SIM} caused by a corresponding increase in the

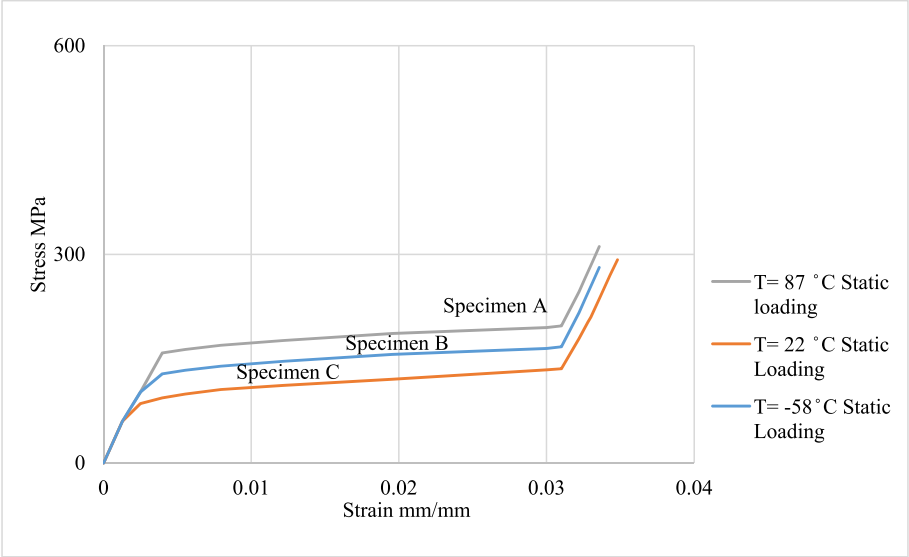

Fig. 7. The stress-strain curves showing maximal tension stresses "C-shaped" NiTi actuator during quasi-static loading (1.3 N) at T = 87 °C, 22 °C and −58 °C (M_s ˂ T˂ A_s).

loading temperature, including the increase related to the transformation heat, typically leads to a decrease in the transformation strain. The geometry of the "C-shaped" actuator is shown schematically in Fig. 5. The neutral axis of the wire is assumed to be overlapping with the center axis of the wire. This wire is bent to the starting "C shape" at T > 600 °C and then is cooled down to room temperature, which results in zero stress at the initial state, as schematically shown in Fig. 5a. However, when the "C-shaped element" is subsequently loaded by 1.3 N, the maximum tension stresses are generated in the volume adjacent to the internal diameter ID and stress gradually reduces towards the centerline of the wire. The maximum compression stresses are concentrated in the volume adjacent to the external diameter OD, as is schematically shown in Fig. 5b. During the strain-recovery process, when heating the wire above A_f^σ temperature, the stress profile of the "C-shaped element" exhibits the opposite "trend" in terms of maximum tension and compression, as is schematically shown in Fig. 5c. The "reversed macroscopic" shape (Fig. 5c) is ideally the same as the macroscopic shape in the initial stage (Fig. 5a), but that is not necessarily true in all cases. The strain-recovery process may show a small amount of unrecovered strain, depending on the amount of the plastic deformation during the loading process.

After cooling from the austinite phase, a quasi-static loading at temperature $T_{SIM} = M_s + \Delta T_I$ is applied to the three fully austenitic samples (A, B, C). Upon the applied load, they are deformed, and part of their volume reaches critical stress σ_{SIM}. For the sake of simplicity and clarification, only specimen B is used as an example to discuss the first thermomechanical cycle on the strain-temperature diagram (Fig. 6).

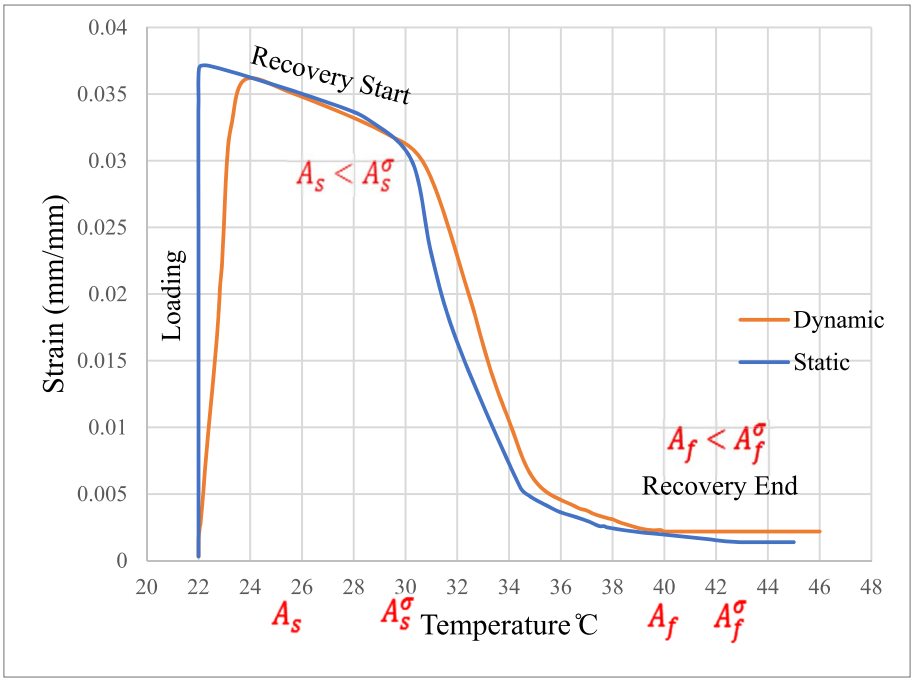

Fig. 8. The temperature-strain curves' comparison of "C-shaped" NiTi wire during static and dynamic loadings and strain recovery process in the stress-induced martensite scenario.

Specimen B is loaded at 22 °C by a "slow deformation process" with no temperature increase during the loading phase, except at the phase transformation, which includes heat generation. This heat is absorbed by an ambient atmosphere at a sufficiently high rate; therefore, the whole loading process can be considered isothermal, as shown in Fig. 6. No incline can be seen in the strain-temperature dependence during loading. During the heating process, at a constant applied external stress, sample B reaches A_s^σ temperature at the beginning of the strain recovery. The applied model predicts $A_s^\sigma = 30$ °C, which is higher than the initial A_s (25 °C), as shown in Fig. 6 (recovery start part). The strain recovery process continues upon further increase of temperature and is completed after sample B reaches temperature A_f^σ (43 °C), which is again higher than the A_f temperature (40 °C) characteristic for complete phase transformation when no external stress is applied. The modeled thermomechanical cycle on the strain -temperature diagram (Fig. 6) shows that most of the applied strain has been recovered upon heating to T> A_f^σ. Nevertheless, there is a small amount of nonrecoverable strain, which is related to the small plastic deformation that was generated during the phase transformation.

For a comparison and demonstration of the effects of chemistry and treatment history, Fig. 7 shows the stress-strain curves for the "C -shaped" samples subjected to 1.3 N load at T = 88 °C, 22 °C and −58 °C (M_s ˂ T˂ A_s) for all three alloys A, B and C, respectively. Note that the dependences shown in Fig. 7 represent the maximum stresses that occur only in limited volume (see Fig. 5) of the loaded "C-shaped" samples. In the quasi-static loading scenario, the "elastic modulus" or stiffness of specimen A is higher than the stiffness of specimens B and C. In addition, after reaching critical stress, the observed "hardening" is similar, and no clear change of the stress-strain slope is predicted by the model when the three specimens are compared. Interestingly, the model also predicted that the elastic straining of the martensitic phase follows the transformation plasticity and represents "elastic moduli" of determined martensite in three A, B and C alloys. The stress-strain dependence shows a similar trend during loading at different temperatures. Nevertheless, the predicted stress levels for plateaus increase with the increasing loading temperature (T_{SIM}=M_s + ΔT_1), although ΔT was identical.

3.2. Dynamic loading, stress-induced martensite transformation scenario

The major difference, when comparing this dynamic SIM scenario to the static SIM loading scenario, is the fact that the heat convection effect is not effective, and the quickly loaded element does not cool sufficiently enough. The generated transformation heat is not effectively conducted away, and the "C-shaped" element is heated. This effect of the transformation enthalpy leads to an increase of the temperature and an increase of the critical stress σ_{SIM} required for martensitic formation in the remaining, but not yet transformed, volume of the "C-shaped" element. In this case, specimen B is initially loaded at 22 °C, but the temperature increases in the loading phase. As a consequence, the whole process can be considered to be adiabatic, which, as shown in Fig. 8 (loading part), leads to an incline in the initial strain-temperature dependence, which is represented by the blue curve. To show the difference between dynamic loading and the previous static loading during the "stress-induced martensite scenario," the two corresponding curves are plotted in Fig. 8. During the strain recovery process at constant stress, the dynamically loaded sample B reaches A_s^σ temperature (31 °C), which is, again, higher than the A_s^σ temperature (30 °C) in static loading, as shown in Fig. 8, and the "C-shaped" element starts to recover. The strain recovery process ends when sample B reaches A_f^σ (44 °C), which is higher than the A_f^σ temperature (43 °C) characteristic for static loading. Clearly, the adopted model confirms differences in the transformation temperaturesA_s^σ ,A_f^σ between dynamic and static loading. Fig. 8 also shows that the higher recoverable strain of the NiTi element is typical for the static loading scenario. This is because lower plastic deformation is generated during static loading than during dynamic loading. However, a certain small amount of strain has not been recovered upon heating to T> A_f^σ in both compared situations.

The maximum stress and strain during the loading stage occur in the volume adjacent to the ID "the inside surface" of "C- shaped" specimens, as marked by arrows in Figs. 9 and 10, respectively, for specimen B. It is very clear that the stress and strain are nonhomogenously distributed in the wire volume. However, the major part of the stressed volume of the "C-shaped" element "passed the critical stress" for SIM phase transformation. This stress level is sufficient to form the preferentially oriented martensite and to generate the required orientation strain, as well as the recovery stress, upon subsequent heating above A_f^σ.

It is also important to mention that during the strain recovery stage (reverse movement), the generated maximum compression stress concentrates in the volume adjacent to the wire's "inner surface" (ID). This stress is higher than the generated tension stress, which concentrates in the volume adjacent to the outer diameter "outside surface" (OD) of the wire, as shown in Figs. 11 and 12, respectively. This model provides clear evidence of the "C-shaped" NiTi asymmetric behavior in tension and compression in terms of the maximum stress and strain values detected at ID and OD, respectively, during the actuator working cycle.

In the dynamic loading scenario, the predicted "elastic moduli" of specimens A, B and C are higher than the elastic moduli predicted for the same samples subjected to quasi-static loading. The calculated values are shown in Table 2. The slope of predicted σ-ε plateau (or "hardening") is greater than zero and is also higher (see Fig. 13) when compared to the static loading scenario (see Fig. 7). The dynamically loaded sample requires a continuous increase in the stress value due to a temperature increase resulting from ongoing phase transformation. The recoverable strain and the extent of memory element motion decreased in a

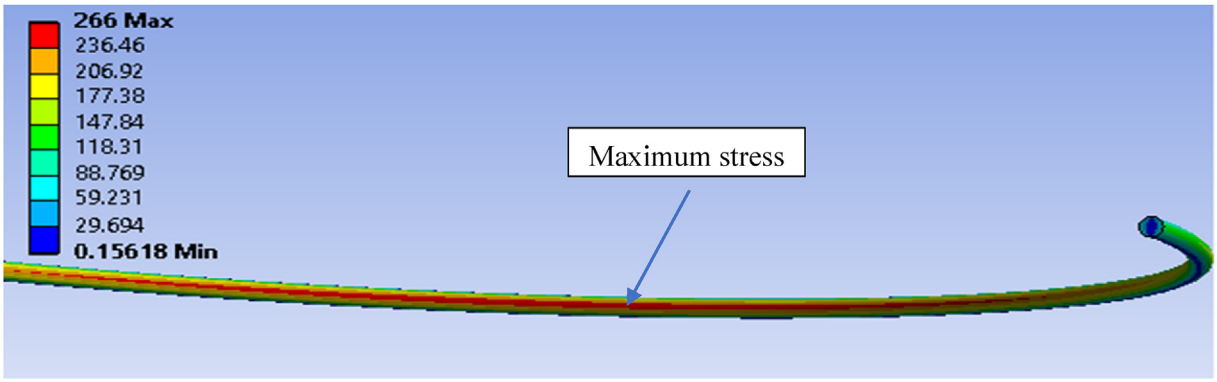

Fig. 9. An example of uneven stress distribution showing its maximum in the volume adjacent to the inner diameter (ID) of the "C-shaped" NiTi element (specimen B loaded with 1.3 N at M_s˂ T˂ $A_s$after cooling from above A_f).

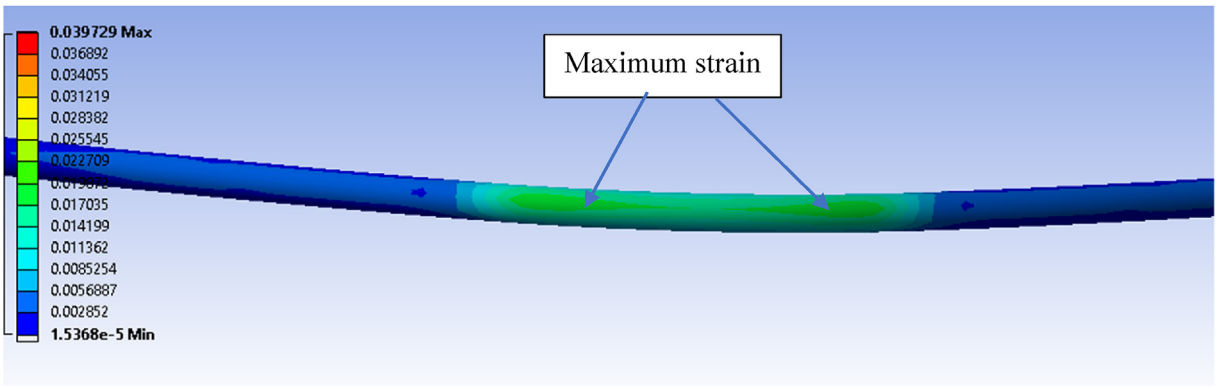

Fig. 10. An example of uneven strain distribution showing the maximum in the volume adjacent to the inner diameter (ID) of the "C-shaped" NiTi element (specimen B loaded with 1.3 N at M_s˂ T˂ A_s after cooling from above A_f).

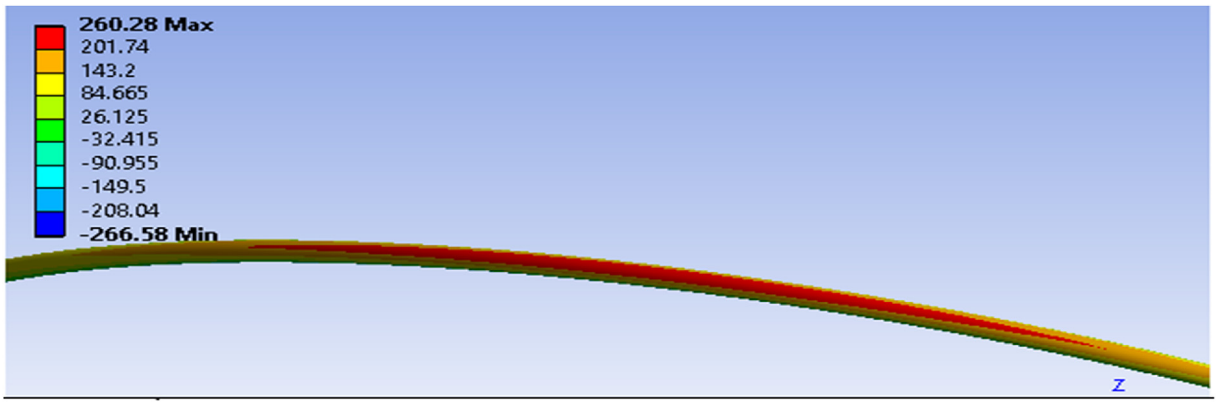

Fig. 11. Tension stress distribution showing the maximum in the volume adjacent to the outer diameter (OD) of the "C-shaped" element generated during reverse movement T ˃ A_f^{σ}.

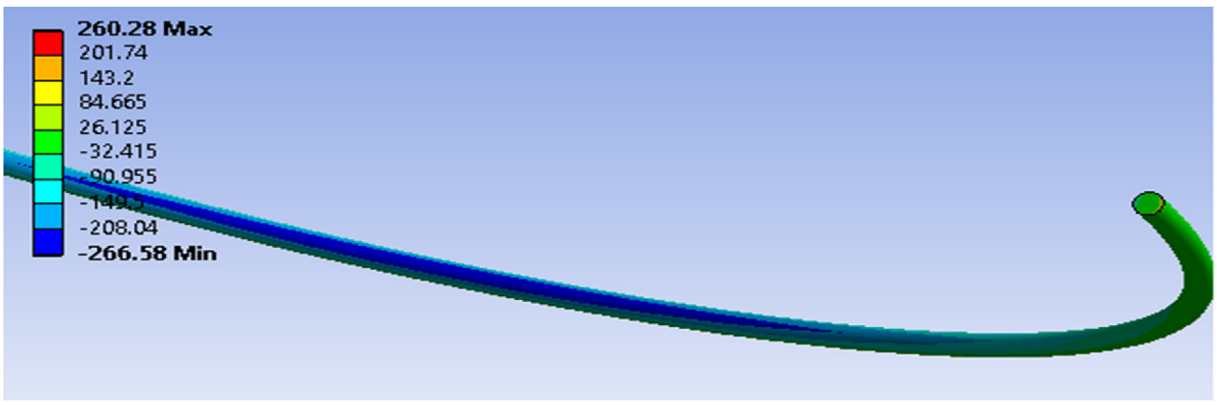

Fig. 12. Compression stress distribution showing the maximum in the volume adjacent to the inner diameter (ID) of the "C-shaped" wire generated during reverse movement upon heating to T ˃A_f^{σ}.

dynamically loaded element when compared with the quasi-static loading case.

Table 2
"Elastic moduli" calculated for different samples and two loading scenarios.

		Static	Dynamic
E (MPa)	A	37.5	43
E (MPa)	B	32	37
E (MPa)	C	24	28

3.3. Quasi-static loading with reorientation of the martensitic variants

In this case, the "C-shaped" memory element is initially in a fully martensitic state with the martensite variants in a self-accommodated arrangement having different orientations [8]. The self-accommodated microstructure of three different samples A, B, and C. is then loaded by applying 1.3 N at three different temperatures $T_R = M_f - \Delta T_{II}$. In all cases, the initially elastic deformation is followed by reorientation-related "plasticity" after the applied load reaches the value of critical stress σ_M^r(Fig. 1). As obvious in Fig. 3, the critical reorientation

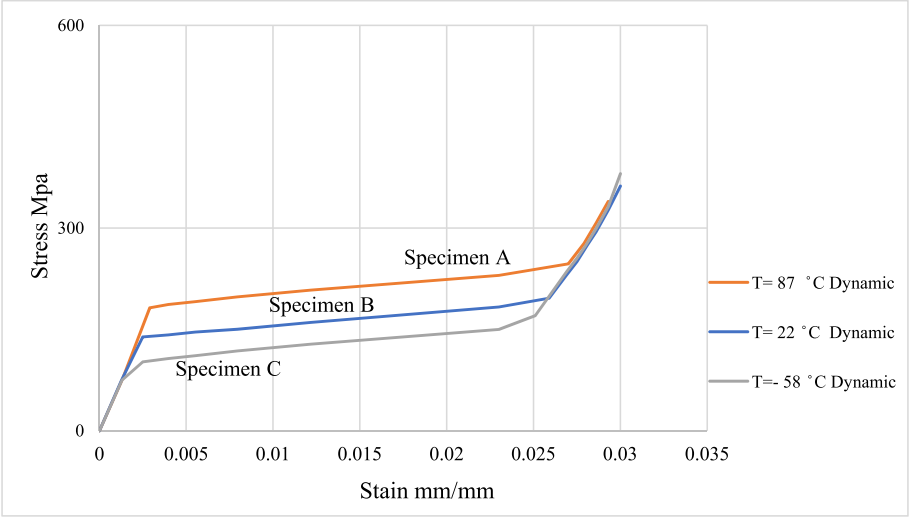

Fig. 13. The stress-strain curves of three different "C-shaped" NiTi memory elements during dynamic loading at (M_s˂ T˂ A_s).

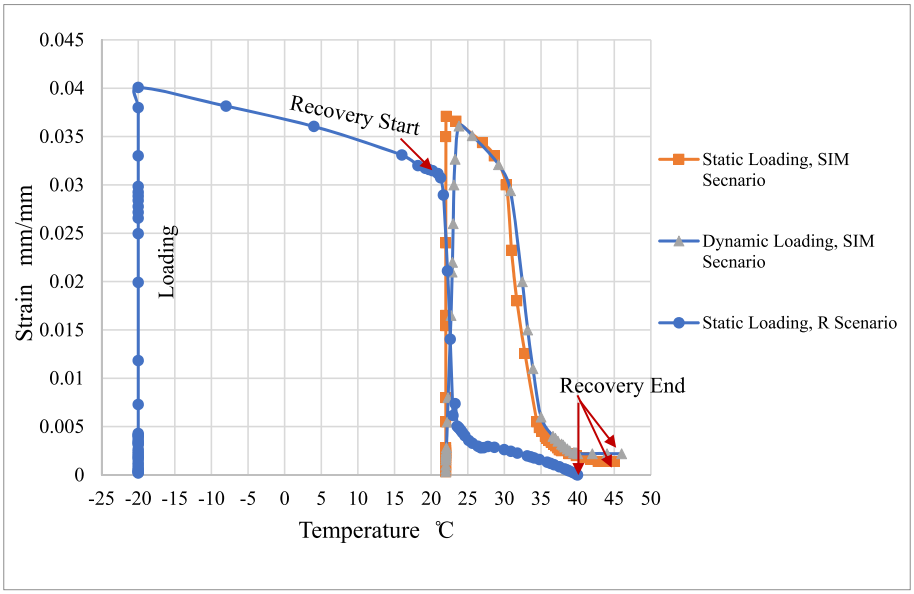

Fig. 14. The calculated temperature-strain curves of the "C-shaped" NiTi elements showing loading and strain recovery process for different types of loading and scenarios.

process starts at consecutively lower stresses (is much easier), when loading occurs closer to the austenite start temperature [6]. This process would require less mechanical energy to deform the wire. No transformation is heat generated, as there is no phase transformation, and the movement of different variant boundaries can be considered to be "frictionless" [2]. When loading specimen B, the whole process can be considered to be isothermal, which is represented by the loading part of the plot in Fig. 14. As also shown in Fig. 14, the beginning of the strain recovery process starts when sample B reaches A_s^σ temperature 27 °C which is only slightly higher than the A_s temperature (25 °C). The A_s - A_s^σdifference is larger in the stress-induced scenario compared to the reorientation scenario.

The strain recovery process ends when sample B reaches A_f^σ (41° C), which is only slightly higher than the A_f temperature (40 °C). Obviously, this value is again lower than the A_f^σ temperatures calculated for the stress-induced martensite scenario (43 or 44 °C). It can be concluded that loading in the reorientation scenario represents the most efficient method of operation for low "shifting" of transformation temperatures.

Fig. 14 also shows that when heating the NiTi samples above A_f, the samples that were subjected statically and dynamically to a reorientation scenario completely recover their shape after heating above A_f^σ, while stress-induced scenario samples always exhibit nonrecoverable deformation.

Fig. 15 shows the stress-strain curves resulting from bending load applied at T = 40 °C, −20 °C and −100 °C ($T_R = M_f - \Delta T_{II}$) for specimens A, B and C, respectively. Note that the maximum stress is not achieved in the entire volume of the "C-shaped" memory element, as discussed earlier. The elastic straining, followed by reorientation plasticity, to almost identical stiffness is seen by the σ-ε slope for each loading rate. As is apparent from Fig. 14, the stress plateau increases with the decreasing loading temperature $T_R = M_f - \Delta T_{II}$of each specimen, although the ΔT was identical for all three compared samples A, B and C.

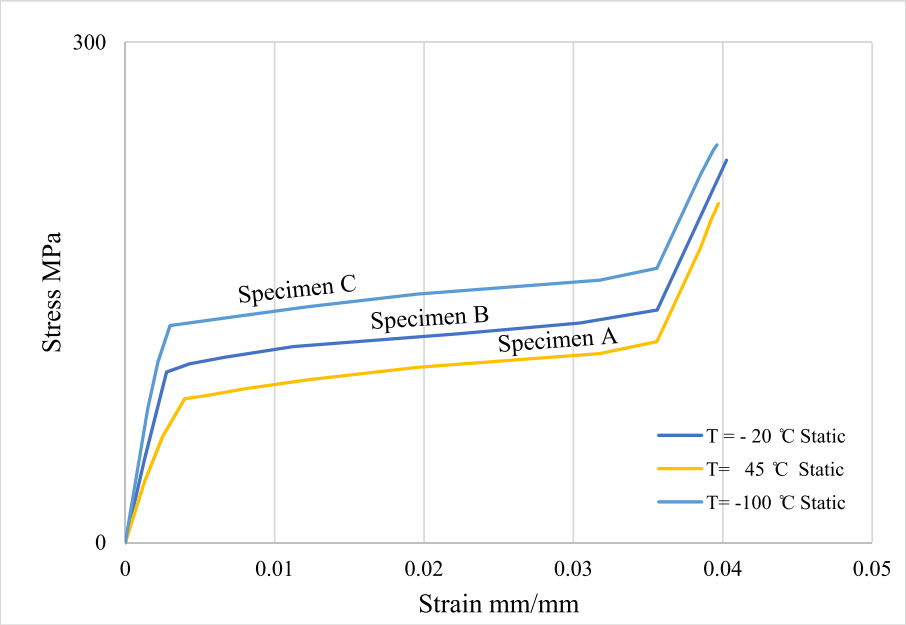

Fig. 15. The stress-strain curves of "C- shaped" NiTi elements during quasi-static loading at temperature T_R.

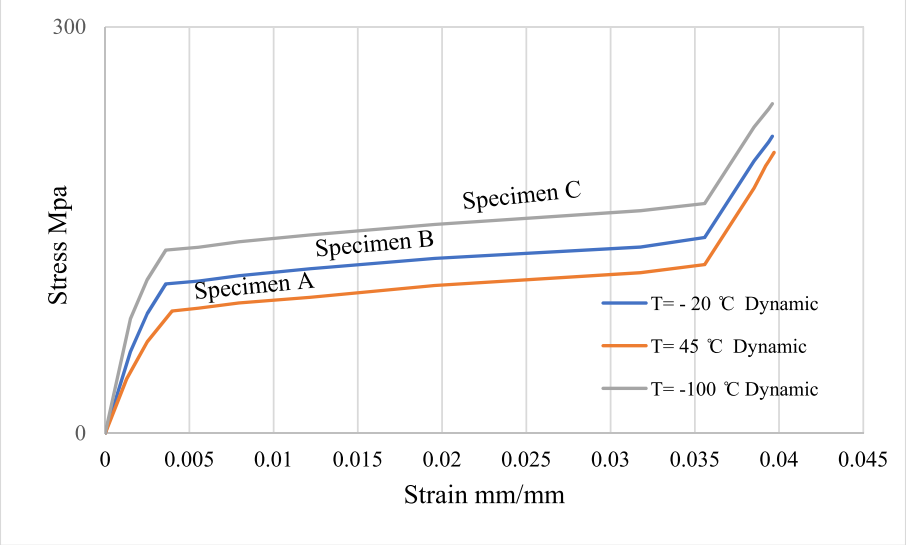

Fig. 16. The stress-strain curves of "C-shaped" NiTi element during dynamic loading at temperature T_R.

3.4. Dynamic loading with reorientation of martensitic Variants (No phase transformation)

In this case, the "C-shaped" element is in a fully martensitic state with the martensite variants in a self-accommodated arrangement obtained with different orientations after cooling of free standing (unloaded) elements to $T_R = M_f - \Delta T_{II}$ [8]. The same boundary conditions as for the static loading "reorientation scenario" were applied. As discussed earlier, the model assumes that during "fast" dynamic loading of the "C-shaped" element, the temperature remains constant, since the reorientation process does not generate heat [2]. The resulting model of thermomechanical behavior is given in Fig. 16 and is similar to the quasi-static loading reorientation scenario behavior shown in Fig. 15. The strain-temperature diagram characteristic for this dynamic loading reorientation scenario is also similar to the strain-temperature diagram in static loading.

The maximum stress and strain distribution adjacent to the inner surface ID of specimen B is shown in Figs. 17 and 18, respectively. Obviously, the stress and strain contours are nonhomogenously distributed in the entire volume of the loaded element. However, part of the element volume reached the critical stress level σ_M^r or higher.

3.5. The macroscopic displacements of the NiTi elements for the two scenarios

For the sake of comparison between the modeled scenarios seen in the sample B, the macroscopic displacement of "C-shaped" shape memory elements loaded by 1.3 N at $T_{SIM} = M_s + \Delta T_I$ *or at* $T_R = M_f - \Delta T_{II}$ and subsequently heated to T° A_f^σ, is presented in Fig. 19. The macroscopic displacement of 57 mm can be reached during loading and for the SIM scenario. For the element subjected to the dynamic loading in the SIM scenario, the recoverable displacement is 54.5 mm. As discussed above, an incomplete recovery was modeled due to plasticity and inhomogeneous stress distribution. In addition, the lower stress loading could also be achieved in the SIM scenario at point 6 in Fig. 3. A full recovery has

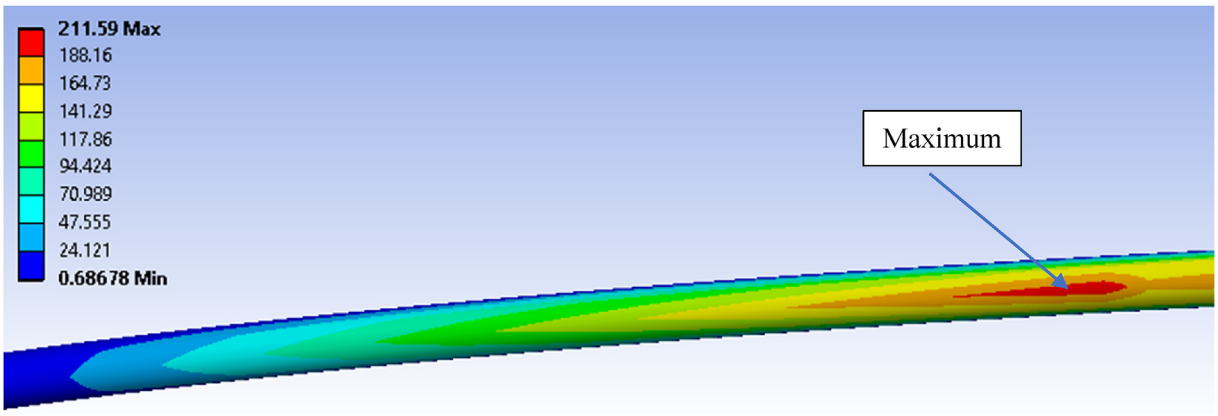

Fig. 17. Inhomogeneous stress distribution with the maximum stress levels obtained in the volume adjacent to the inner diameter (ID) of the "C-shaped" NiTi element B loaded at T_R.

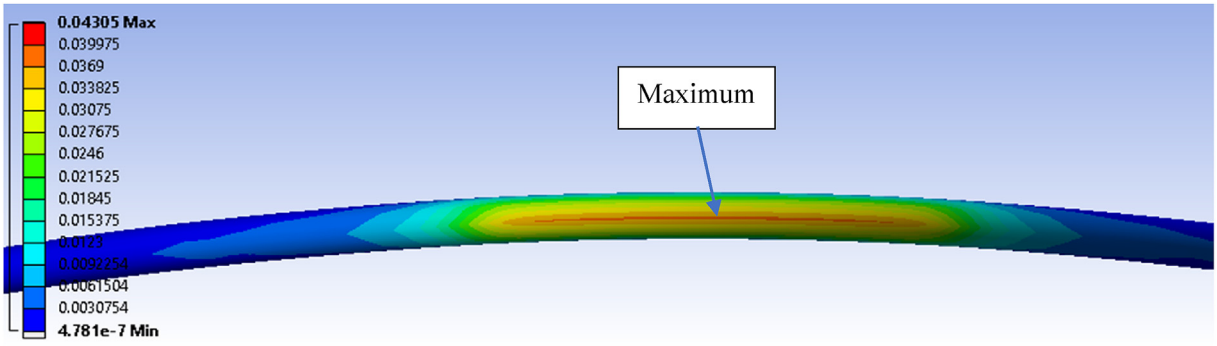

Fig. 18. Inhomogeneous strain distribution with the maximum strain levels obtained in the volume adjacent to the inner diameter (ID) of the "C-shaped" NiTi element B loaded at T_R.

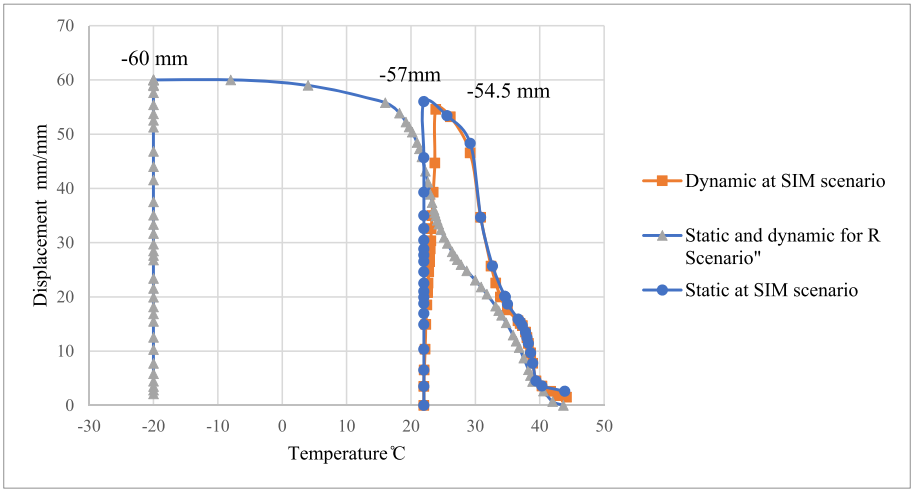

Fig. 19. The macroscopic displacement-temperature curve of "C-shaped" NiTi element B loaded at different scenarios (SIM-stress -induced martensite scenario, R-reorientation scenario).

Table 3
The transformation temperatures for the commercial NiTi sample as received condition provided by FIBRA Ltd.

Ti-x at. % Ni	M_f(°C)	M_s(°C)	A_s(°C)	A_f(°C)
50	**−10.1**	**13.5**	**31**	**45**

been achieved when the element is deformed at a lower critical stress typical for the reorientation scenario. The highest recoverable macroscopic displacement of 60 mm is seen here.

We also believe that the simple tensile test data of those structures with defects can give us a necessary data for that model with respect to slope, critical stress and recovery strain.

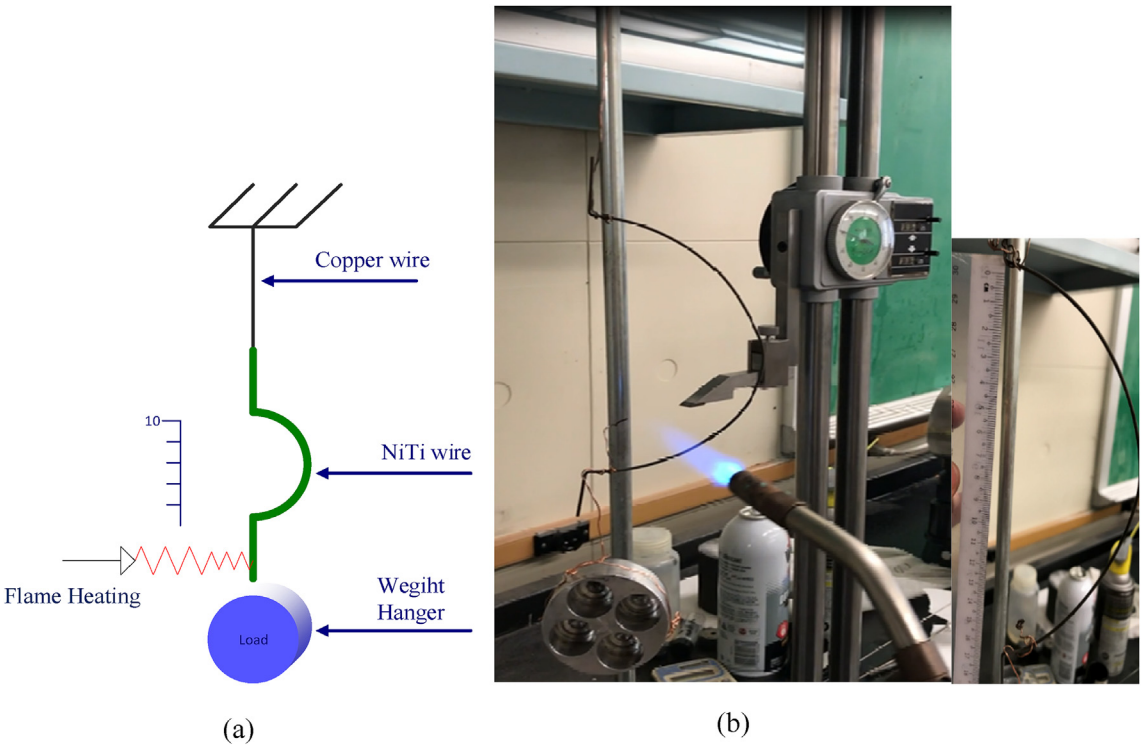

Fig. 20. Thermomechanical loading of the "C-shape" NiTi wire test setup (a) Schematic (b) Real Picture.

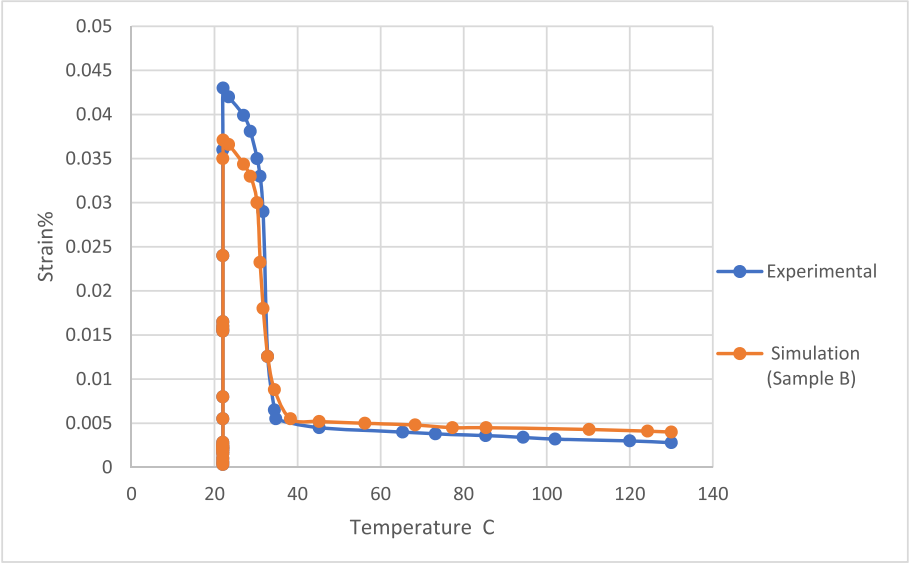

Fig. 21. The recoverable strain measurements obtained by Ansys Workbench 18.2. and compared with the experimental results of the "C-shaped" NiTi wire (sample B) as mechanically loaded for 128.5 g at 22 °C, followed by heating to temperature 130 °C.

4. Experimental validation

The commercial NiTi material that was provided by FIBRA Ltd./ Check Republic was used in the thermomechanical test and used for comparison with sample B for simplicity purposes. The transformation temperatures and the chemical compositions of the NiTi commercial sample are listed in Table 3. Fig. 20 a and b show the schematic and the actual picture of the test setup where the NiTi "C-shaped" wire was loaded by a constant weight at the lower end and was supported by the copper wire at the upper end. The purpose of the thermomechanical loading experiment was to determine whether the displacement-temperature response of NiTi wire subjected to the consecutive thermomechanical load (128.5 g) followed by heating. More details about the experimental work will be found in Ref. [22].

The thermomechanical test was carried out at room temperature, 22 °C, which was above the M_s temperature when the "C-shaped" NiTi wire was in the austinite state. This means that only the high strain rates in SIM scenario were considered for comparison and estimated from the strain rate equation (ΔL/L/t). The recoverable strain of the "C-shaped" NiTi wire was measured after loading, was compared with the simulation results and showed good agreement, as shown in Fig. 21.

5. Conclusions

Transient numerical simulation using finite element analysis FEA in Ansys 18.2 allows the investigation of thermomechanical behavior related to dynamic and quasi-static loading of NiTi elements exhibiting a shape memory effect.

1. The uniaxial tensile test parameters obtained for NiTi SMAs with different chemistry and thermomechanical treatment were used in models simulating "memory actuator" behavior applied at different loading scenarios. The developed model predicts the different behaviors of NiTi alloy for both scenarios in the first thermomechanical cycle and their similarity in the second thermomechanical cycle. The adopted data reflecting the impact of thermomechanical treatment on the stress-strain and temperature-displacement behavior of NiTi alloy.
2. If the developed transient thermal-structure modeling performed and the data which were generated by tensile tests were used, the model works. This data reflects the microstructure changes "i.e. work hardened, annealed" and their impact on the stress-strain and temperature-displacement behavior of NiTi alloy which are quite often omitted in different models.
3. The macroscopic displacement of "C-shaped" NiTi elements during the loading process in reorientation scenarios is higher than the macroscopic displacements in the SIM scenario during both static and dynamic loadings.
4. The elements loaded in the reorientation scenario exhibit full recovery of deformation, while the SIM scenario is typified by residual unrecoverable deformation.
5. Better recovery parameters, in terms of maximum recoverable strain as well as maximum capacity to reverse these strains upon heating, were obtained for elements loaded at lower levels of critical stresses necessary for the onset of plateaus in σ-ε dependences.
6. Loading speed and subsequent adiabatic effects causing temperature increases can have a significant impact on recoverable strains.
7. Inhomogeneity of stresses and deformations within the volume of loaded elements can lead to irreversible plastic deformation.
8. The transient thermal structural analysis has shown that in the case of static loading during stress-induced martensite scenarios, the "elastic moduli" and the critical stress values σ_{SIM} necessary for macroscopic deformation are lower than their corresponding stress levels required in the case of dynamic loading.
9. For the SIM scenario, the recoverable strain of "C-shaped" memory elements subjected to dynamic loading is lower than the recoverable strain typical for the element subjected to the quasi-static loading.
10. The recovery strain value in both scenarios depends on the type of loading (i.e., dynamic or static) and on the initial microstructure (i.e., austenite or martensite).
11. The transient thermal structural analysis has shown that in the reorientation martensite scenario, the thermomechanical behavior of "C-shaped" NiTi memory elements is similar during static and dynamic loading, as there is no transformation heat effect in either case.

Acknowledgment

This work has been a combined effort between the department of Mechanical Engineering and Energy Processes at Southern Illinois University and the Mechanical Engineering Department of the University of Diyala. The author would like to acknowledge those departments for their hard work and dedication of the research and its development. Additionally, the author would like to acknowledge the support and funding of the University of Diyala for enabling this continued research.

References

[1] J. Mohd Jani, et al., A review of shape memory alloy research, applications and opportunities, Mater. Des. 56 (2014) 1078–1113.
[2] M.H. Elahinia, Shape Memory Alloy Actuators : Design, Fabrication, and Experimental Evaluation. 2015, John Wiley & Sons, Ltd., Chichester, West Sussex, 2016.
[3] C. Morin, Z. Moumni, W. Zaki, Thermomechanical Coupling in Shape Memory Alloys under Cyclic Loadings: Experimental Analysis and Constitutive Modeling, Elsevier Science B.V., Amsterdam.: Great Britain, 2011, p. 1959.
[4] A. Alipour, M. Kadkhodaei, A. Ghaei, Finite element simulation of shape memory alloy wires using a user material subroutine: parametric study on heating rate, conductivity, and heat convection, J. Intell. Mater. Syst. Struct. 26 (5) (2015) 554–572.
[5] L. Fumagalli, F. Butera, A. Coda, SmartFlex® NiTi wires for shape memory actuators, J. Mater. Eng. Perform. 18 (5/6) (2009) 691–695.
[6] P. Filip, Titanium-nickel shape memory alloys in medical applications, in: Titanium in Medicine, Springer, 2001, pp. 53–86.
[7] J.M.G. Fuentes, P. Gumpel, J. Strittmatter, Phase Change Behavior of Nitinol Shape Memory Alloys, WILEY VCH, Germany, 2002, p. 437.
[8] P. Filip, K. Mazanec, Letter, Influence of work hardening on the reactive stress in a TiNi shape memory alloy, Mater. Sci. Eng. A 174 (1994) L41–L43.
[9] R. Mirzaeifar, R. DesRoches, A. Yavari, Analysis of the rate-dependent coupled thermo-mechanical response of shape memory alloy bars and wires in tension, Continuum Mech. Therm. 23 (4) (2011) 363–385.
[10] F. Auricchio, E. Sacco, Thermo-mechanical modelling of a superelastic shape-memory wire under cyclic stretching–bending loadings, Int. J. Solids Struct. 38 (2001) 6123–6145.
[11] D.C. Lagoudas, et al., Dynamic Loading of Polycrystalline Shape Memory Alloy Rods, Elsevier Science B.V., Amsterdam.: Netherlands, 2003, p. 689.
[12] F. Auricchio, D. Fugazza, R. Desroches, Rate-dependent thermo-mechanical modelling of superelastic shape-memory alloys for seismic applications, J. Intell. Mater. Syst. Struct. 19 (1) (2007) 47–61.
[13] J. McCormick, et al., Structural engineering with NiTi. II: mechanical behavior and scaling, J. Eng. Mech. 133 (9) (2007) 1019–1029.
[14] S. Nemat-Nasser, W.-G. Guo, Superelastic and cyclic response of NiTi SMA at various strain rates and temperatures, Mech. Mater. 38 (5–6) (2006) 463–474.
[15] C. Grabe, O.T. Bruhns, On the viscous and strain rate dependent behavior of polycrystalline NiTi, Int. J. Solids Struct. 45 (7–8) (2008) 1876–1895.
[16] Y.J. He, Q.P. Sun, Rate-dependent domain spacing in a stretched NiTi strip, Int. J. Solids Struct. 47 (20) (2010) 2775–2783.
[17] D. Depriester, et al., Thermomechanical modelling of a NiTi SMA sample submitted to displacement-controlled tensile test, Int. J. Solids Struct. 51 (10) (2014) 1901–1922.
[18] H. Yu, M.L. Young, Three-dimensional modeling for deformation of austenitic NiTi shape memory alloys under high strain rate, Smart Mater. Struct. 27 (1) (2018), 015031.
[19] D. Roche, M. Senousy, Coupled Field Physics Version 1.2, Ansys Inc., 2017.
[20] J. Arghavani, F. Auricchio, R. Naghdabadi, A finite strain kinematic hardening constitutive model based on Hencky strain: general framework, solution algorithm and application to shape memory alloys, Int. J. Plast. 27 (6) (2011) 940–961.
[21] MateWeb, L. 2019 [cited 2019 01/03/2019]; Available from: www.matweb.com.
[22] S. Alazzawi, P. Filip, Designing a Smart Greenhouse Ventilation Window Based on NiTi SMA Actuator, Doctorate Dissertation, SIUC, USA, 2019.